



# Electrochemical performance of Al<sub>2</sub>O<sub>3</sub> pre-coated spinel LiMn<sub>2</sub>O<sub>4</sub>

Hong-Ming Zhou\*, Yu-Hua Zhu, Jian Li,  
Wen-Jiao Sun, Zhong-Zhong Liu

Received: 28 November 2013 / Revised: 24 December 2013 / Accepted: 26 November 2014 / Published online: 4 January 2015  
© The Author(s) 2015. This article is published with open access at Springerlink.com

**Abstract** Al<sub>2</sub>O<sub>3</sub>-coated spinel LiMn<sub>2</sub>O<sub>4</sub> cathode materials, presintered LiMn<sub>2</sub>O<sub>4</sub> (P-LMO), and calcined LiMn<sub>2</sub>O<sub>4</sub> (C-LMO) were synthesized by chemical deposition and thermal treating method using presintered and calcined LiMn<sub>2</sub>O<sub>4</sub> as precursors. The crystal structure, morphology, the thickness of the coating layer, and particle size of prepared samples were investigated by X-ray diffraction (XRD), scanning electron microscopy (SEM), high-resolution transmission electron microscopy (HRTEM), and Malvern instruments. The average particle size of P-LMO with like-spheres (0.3 μm) is much smaller than that of C-LMO (0.5 μm). The Al<sub>2</sub>O<sub>3</sub> layer of P-LMO can effectively reduce the charge transfer resistance and inhibit the Mn dissolution. The electrochemical performance of P-LMO is better than that of C-LMO. It is found that the LiMn<sub>2</sub>O<sub>4</sub> cathode materials have excellent electrochemical cyclability by coated 2 mol% Al<sub>2</sub>O<sub>3</sub> at the surface of presintered material. The initial discharge capacity of the material with 2 mol% Al<sub>2</sub>O<sub>3</sub>-coated is 114.0 mAh·g<sup>-1</sup> at 0.1C rate and 55 °C, and the capacity retention is 87.3 % at 0.5C rate.

**Keywords** Cathode materials; Lithium manganese oxide; Pre-coated; Aluminum oxide; Cycling stability

## 1 Introduction

Spinel LiMn<sub>2</sub>O<sub>4</sub>, owing to its easy preparation, economic, and environmental advantages, is considered to be a promising material for the positive electrode of secondary lithium batteries [1–3]. The compound has significant advantages in terms of toxicity and cost over LiCoO<sub>2</sub>. Moreover, the natural abundance of manganese and the familiarity of battery manufacturer with the chemistry of manganese oxides, used in primary alkaline cells [4], made the choice of LiMn<sub>2</sub>O<sub>4</sub> even more attractive.

The capacity of spinel LiMn<sub>2</sub>O<sub>4</sub>, however, fades rapidly during charge/discharge cycling, which seriously hinders the commercial application of spinel LiMn<sub>2</sub>O<sub>4</sub> materials. Several possible reasons were proposed to contribute to this fading, such as Jahn–Teller distortion [5], dissolution of spinel into the electrolyte, and decomposition of the electrolyte [6] during cycling and oxygen loss from the spinel lattice of cathode material [7]. Extensive studies were directed toward various strategies to overcome the capacity fading problem of LiMn<sub>2</sub>O<sub>4</sub>. Elemental substitution of Mn with transition metals, such as Zr, Co, Al, Cr, Ni, Mg, etc. [8–12], was proven to be an effective method. However, the improved capacity retention is usually realized at the expense of the decrease of specific capacity.

Morphology, surface chemistry, surface species of the cathodes and the interface between cathodes and electrolyte are of great importance to the electrochemical performance of lithium-ion batteries. Oxides such as MgO, TiO<sub>2</sub>, CeO<sub>2</sub>, ZnO, ZrO<sub>2</sub>, and Al<sub>2</sub>O<sub>3</sub> [13–17], were studied to suppress capacity fading, indicating that the effectiveness of surface modification on spinel LiMn<sub>2</sub>O<sub>4</sub>. Al<sub>2</sub>O<sub>3</sub> was improved to be one of the surface coating materials for lithium-ion batteries because of its various advantages such as low cost, excellent chemical stability, and high

H.-M. Zhou\*, Y.-H. Zhu, J. Li, W.-J. Sun, Z.-Z. Liu  
School of Materials Science and Engineering, Central South University, Changsha 410083, China  
e-mail: ipezhm@163.com

H.-M. Zhou, J. Li  
Hunan Zhengyuan Institute for Energy Storage Materials and Devices, Changsha 410083, China

electronic conductivity possessed by amphoteric oxides [18]. Currently, most of the studies focus on the coating methods of Al<sub>2</sub>O<sub>3</sub>. Tu et al. [19] reported that the Al<sub>2</sub>O<sub>3</sub> layer was coated through a melting impregnation method, and Kim et al. [20] found Al<sub>2</sub>O<sub>3</sub> could coat on the spinel LiMn<sub>2</sub>O<sub>4</sub> by electrostatic attraction forces. On the basis of preliminary studies, Al(OH)<sub>3</sub> layer was prepared on the surface of presintered LiMn<sub>2</sub>O<sub>4</sub> by a chemical deposition method, and then it was thermally treated to form Al<sub>2</sub>O<sub>3</sub> layer. The Al<sub>2</sub>O<sub>3</sub> layer can inhibit the growth of LiMn<sub>2</sub>O<sub>4</sub> during the progress of calcination and reduce the particle size. Moreover, the layer can effectively isolate the LiMn<sub>2</sub>O<sub>4</sub> and electrolyte, reduce the contact area and diffusion of Mn in the electrolyte, and further improve the electrochemical performance of spinel LiMn<sub>2</sub>O<sub>4</sub> cathode materials. However, there are few reports on the preparation of Al<sub>2</sub>O<sub>3</sub>-coated LiMn<sub>2</sub>O<sub>4</sub> using the presintered LiMn<sub>2</sub>O<sub>4</sub> as precursor. In this work, presintered LiMn<sub>2</sub>O<sub>4</sub>(P-LMO) and calcined LiMn<sub>2</sub>O<sub>4</sub>(C-LMO) coated with different amounts of Al<sub>2</sub>O<sub>3</sub> were prepared, and the effects of Al<sub>2</sub>O<sub>3</sub> coating on the electrochemical cycling performances of LiMn<sub>2</sub>O<sub>4</sub> were systematically studied.

## 2 Experimental

LiMn<sub>2</sub>O<sub>4</sub> was synthesized by solid-state method. The stoichiometric amounts of Li<sub>2</sub>CO<sub>3</sub> and electrochemically prepared manganese dioxide (EMD) were firstly mixed in ball grinding mill for 16 h. After the mixture was dried at 80 °C, it was sintered at 500 °C for 6 h to obtain presintered LiMn<sub>2</sub>O<sub>4</sub>, and then calcined at 750 °C for 6 h to gain calcined LiMn<sub>2</sub>O<sub>4</sub>.

The Al<sub>2</sub>O<sub>3</sub> coating level was controlled at 2 mol% and 5 mol%, and the preparation process of coating solution was conducted as follows. Certain amounts of presintered LiMn<sub>2</sub>O<sub>4</sub> and calcined LiMn<sub>2</sub>O<sub>4</sub> were homogeneously dispersed in the absolute ethyl alcohol, respectively. The solutions of aluminum nitrate and aqueous ammonia were slowly added into the dispersion successively drop by drop with electromagnetic stirring in a water bath at 80 °C for several hours, and then Al(OH)<sub>3</sub>-coated presintered LiMn<sub>2</sub>O<sub>4</sub> and calcined LiMn<sub>2</sub>O<sub>4</sub> were obtained, respectively, after the solution was evaporated. Finally, the Al(OH)<sub>3</sub>-coated presintered LiMn<sub>2</sub>O<sub>4</sub> and calcined LiMn<sub>2</sub>O<sub>4</sub> powers were annealed in air at 750 and 350 °C for 10 h, respectively, to obtain Al<sub>2</sub>O<sub>3</sub>-coated LiMn<sub>2</sub>O<sub>4</sub>. According to different Al<sub>2</sub>O<sub>3</sub> coating amounts, pristine LiMn<sub>2</sub>O<sub>4</sub>, Al<sub>2</sub>O<sub>3</sub> cal-coated LiMn<sub>2</sub>O<sub>4</sub>, and Al<sub>2</sub>O<sub>3</sub> pre-coated LiMn<sub>2</sub>O<sub>4</sub> were labeled as LMO, C-LMO-2, C-LMO-5, P-LMO-2, and P-LMO-5.

The working electrode was prepared by pressing a mixing of the cathode active material, conductive material (acetylene black), and binder (PVDF) in a weight ratio of

80/10/10. The slurry was then pasted on the aluminum foil current collector and dried at 120 °C under vacuum for overnight. The Li metal was used as the counter and reference electrodes. The electrolyte consisted of 1 mol·L<sup>-1</sup> solution of LiPF<sub>6</sub> dissolved in an ethylene/diethyl carbonate (EC/DEC, 1:1 ratio by volume). The cells were assembled in argon-filled dry box in which both the moisture and the oxygen levels were less than 1 × 10<sup>-6</sup>.

Power X-ray diffraction (XRD, SIEMENS-500) using Cu K $\alpha$  radiation was used to examine the crystalline phase and the evolution lattice parameters of the prepared material. The surface morphology and microstructure of powers were characterized by scanning electron microscopy (SEM, Sirion 200) and high-resolution transmission electron microscopy (HRTEM, JEM-2100F). The distribution of solid particles was determined using a ZetaSizer 3,000 dynamic light scattering instrument (Malvern Inc.). Before electrochemical tests, the batteries were aged for 24 h to ensure good soakage. The cells fabricated were cycled galvanostatically at 0.1C and 0.5C in the potential range of 3.3–4.5V. Alternating current (AC) impedance was carried out by applying frequency of 1 × 10<sup>5</sup>–1 × 10<sup>-2</sup> Hz with ac-amplitude of 5 mV. Cyclic voltammogram (CV) measurements were performed on electrochemical workstation with three electrode systems (CHI660C, Shanghai), and the CV curves were recorded at scan rate of 0.1 mV·s<sup>-1</sup> between 3.3 and 4.5 V (vs. Li/Li<sup>+</sup>).

In order to investigate the effect of Al<sub>2</sub>O<sub>3</sub> coating layer on decreasing the dissolution of cathode material, the Mn dissolution experiment was also carried out in this study according to the method given in Ref. [21]. About 10 mg of LMO, P-LMO, and C-LMO were, respectively, immersed in 10 ml of LiPF<sub>6</sub>-EC/DEC (1 mol·L<sup>-1</sup>, 1:1 volume ratio) electrolyte for 3 days. Then, after separating the cathode material power via filtering through filter paper, the dissolved Mn<sup>2+</sup> in the electrolyte was extracted into water phase using 10 ml HCl (0.1 mol·L<sup>-1</sup>) acid, and the Mn contents were quantitatively determined by atomic absorption spectroscopy (AAS).

## 3 Results and discussion

### 3.1 Physical characterizations

Figure 1 displays the XRD patterns of the LMO, C-LMO, and P-LMO samples with different Al<sub>2</sub>O<sub>3</sub> coating amounts. Figure 1 indicates that all of the diffraction peaks correspond to a well-defined spinel structure with space group *Fd3m*, being in good agreement with JCPDS card 88-1,749. The absence of any other peaks in the patterns indicates that amorphous Al<sub>2</sub>O<sub>3</sub> coating on the surface of the base LiMn<sub>2</sub>O<sub>4</sub> does not penetrate the spinel matrix.

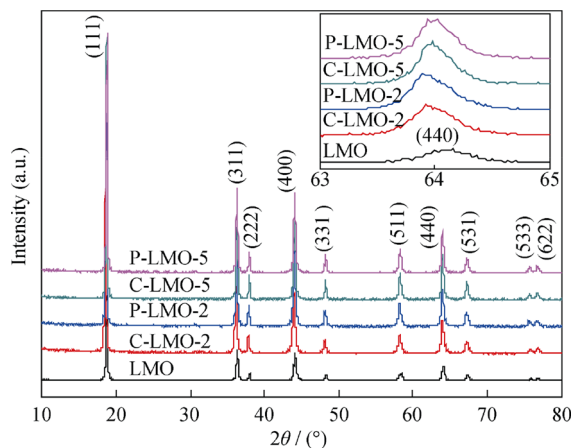


**Fig. 1** XRD patterns of LMO, C-LMO, and P-LMO. Inset showing enlarged diffraction peak of (440)

Compared with the (440) diffraction peak of pristine  $\text{LiMn}_2\text{O}_4$ , as shown in the inset of Fig. 1, all the peaks of the  $\text{Al}_2\text{O}_3$ -coated  $\text{LiMn}_2\text{O}_4$  exhibit a minute leftward shift, demonstrating that the crystal lattice of  $\text{LiMn}_2\text{O}_4$  is enlarged after coating a layer of  $\text{Al}_2\text{O}_3$ . As can be seen from the inset, the lattice constants for both C-LMO and P-LMO increase with the increase of coating amount of  $\text{Al}_2\text{O}_3$ . And for the same amount of  $\text{Al}_2\text{O}_3$  surface-modified spinel  $\text{LiMn}_2\text{O}_4$ , the (440) diffraction peaks of C-LMO have a further leftward than those of P-LMO, which indicates that P-LMO has smaller lattice parameter. So we suggest that the  $\text{Al}_2\text{O}_3$  layer coated at presintering stage can successfully prohibit grain from growing up. Secondary particles are composed of small grains which further confirm the inhibition of  $\text{Al}_2\text{O}_3$  layer to spinel  $\text{LiMn}_2\text{O}_4$ . The particle size measurement of P-LMO-2 and C-LMO-2 was conducted with a laser particle size analyzer.

The particle diameter distributions of P-LMO-2 and C-LMO-2 are presented in Fig. 2. It can be seen from

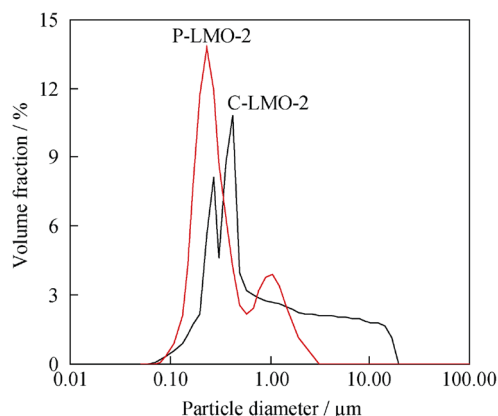


**Fig. 2** Particle diameter distribution of P-LMO-2 and C-LMO-2 powers

Fig. 2 that the average particle sizes of P-LMO and C-LMO are about 0.30 and 0.50  $\mu\text{m}$ , respectively, and the grain size distribution of P-LMO is more concentrated. It may be attributed to the fact that the grain is growing by intergranular annexed to each other and through the migrating of the grain boundary. Because there is a layer of alumina hydroxide coated at the surface of presintered spinel  $\text{LiMn}_2\text{O}_4$  samples before calcinations, the atoms only can grow up in the cladding layer and not by eating grains outside of the cladding layer during the process of calcinations. This is different from the growing way of  $\text{LiMn}_2\text{O}_4$ -coated  $\text{Al}_2\text{O}_3$  after calcinations [22], so the particle diameter of P-LMO is much smaller. This indicates that pre-coated  $\text{Al}_2\text{O}_3$  can reduce the size of particles and also narrow the distribution range of particle size.

The SEM images of the surface morphology of LMO, C-LMO, and P-LMO samples are presented in Fig. 3. The SEM images reveal that the particles of pristine  $\text{LiMn}_2\text{O}_4$  are homogeneously distributed with average particle diameter of 200–300 nm. The border and corner of particles are clearly observed. After surface coating with 2 mol%  $\text{Al}_2\text{O}_3$  (Fig. 3b, c) and 5 mol%  $\text{Al}_2\text{O}_3$  (Fig. 3d, e), the following conclusions can be obtained. Firstly, C-LMO powders exhibit well-developed polyhedral morphology, and the border and corner of the particles are smoother than those of spinel  $\text{LiMn}_2\text{O}_4$ . In contrast, the particle morphology of P-LMO shows spherical shape and the clear border and corner of particles disappear. Secondly, the particle size of P-LMO is smaller than that of C-LMO, which is consistent with the results of particle diameter distribution.

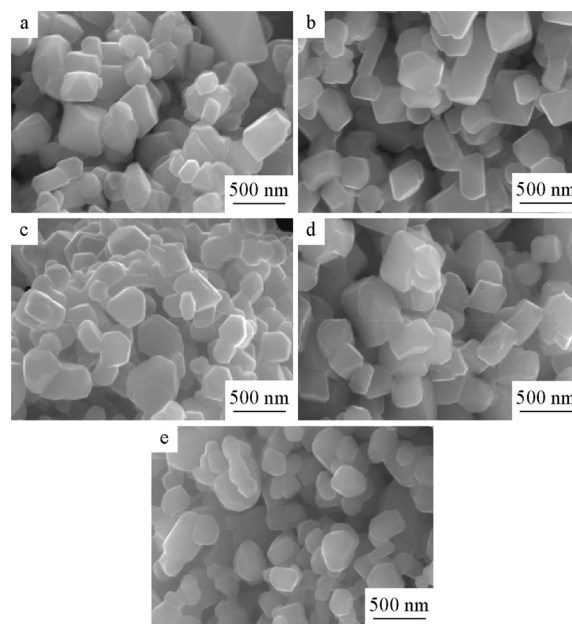


**Fig. 3** SEM images of LMO, C-LMO, and P-LMO powders: a LMO, b C-LMO-2, c P-LMO-2, d C-LMO-5, and e P-LMO-5

HRTEM was applied to characterize what was changed on the particle surface after surface modification. Figure 4 shows the images of LMO, P-LMO-2, and C-LMO-2 particles. From Fig. 4a, it is evident that LiMn<sub>2</sub>O<sub>4</sub> grains are submicron particles with good dispersivity. The average size of these particles ranges from 200 to 300 nm. For both coated samples (Fig. 4b–e), core LiMn<sub>2</sub>O<sub>4</sub> (dark opaque region) can be clearly seen covered by loose thin translucent film. The thickness of the Al<sub>2</sub>O<sub>3</sub> compact coating layer is around 10 nm. No transition layer can be observed, and the interface between the core and coating layer of C-LMO (Fig. 4d) is obvious. However, the interface between the core and coating layer of P-LMO (Fig. 4e) is unobvious. This may be due to that the Al(OH)<sub>3</sub> coating layer of the core presintered LiMn<sub>2</sub>O<sub>4</sub> gradually diffuses into the LiMn<sub>2</sub>O<sub>4</sub> crystal and reacts with it, resulting in the formation of solid solution layer during the sintering process. However, the relative intensity of diffraction peaks has no significant change between LMO and P-LMO, indicating that only a small amount of Al<sup>3+</sup> embed into the crystal on the surface of particles, and then the Li–Al–Mn–O solid solution which is similar to a body-doped LiAl<sub>y</sub>Mn<sub>2-y</sub>O<sub>4</sub> forms on the surface [23].

### 3.2 Electrochemical performance

Figure 5 shows the initial specific discharge capacities of LMO, C-LMO, and P-LMO by applying a current of 0.1C at the potential range of 3.3–4.5 V (vs. Li/Li<sup>+</sup>) at room temperature.

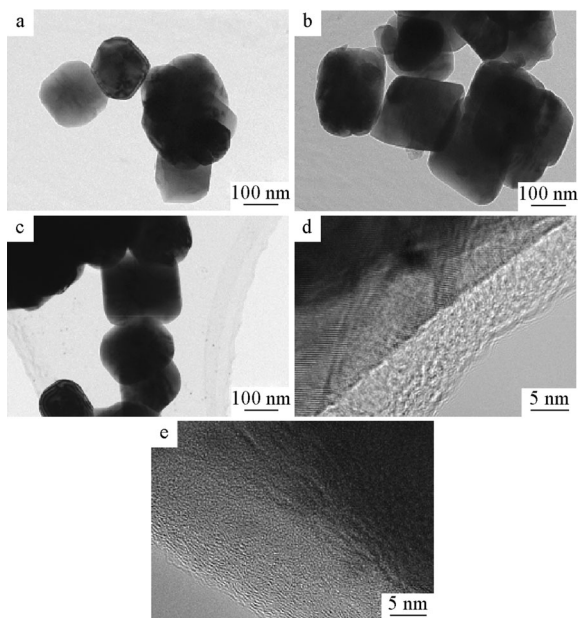


**Fig. 4** TEM images of **a** LMO, **b** and **d** C-LMO-2, **c** and **e** P-LMO-2 powers

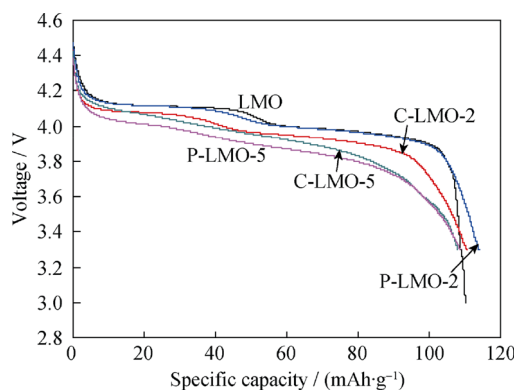


**Fig. 5** Initial specific discharge capacities of LMO, C-LMO, and P-LMO at 0.1C

It can be seen from Fig. 5 that the discharge curves of all samples have two voltage plateaus at approximately 3.9 and 4.1 V. The first plateau at 3.9 V is associated with the single-phase reversible reaction of  $\text{LiMn}_2\text{O}_4 \rightarrow \text{Li}_{0.5}\text{Mn}_2\text{O}_4 + 0.5\text{Li}^+$ , while the second one at 4.1 V is attributed to the two-phase reaction of  $\text{Li}_{0.5}\text{Mn}_2\text{O}_4 \rightarrow \text{Mn}_2\text{O}_4 + 0.5\text{Li}^+$  [21]. The initial discharge capacities of LMO, C-LMO, and P-LMO at room temperature are shown in Table 1. From Table 1, it can be seen that the initial specific discharge capacities of Al<sub>2</sub>O<sub>3</sub>-coated LiMn<sub>2</sub>O<sub>4</sub> are nearly synonymous with that of LMO. This indicates that the layer of Al<sub>2</sub>O<sub>3</sub> has no effect on the initial specific discharge capacity of spinel LiMn<sub>2</sub>O<sub>4</sub>, and a small amount of Al<sup>3+</sup> embedded into the crystal on the surface of P-LMO do not cause the loss of the initial capacity. The two potential plateaus for all P-LMO samples are maintained after 50th cycling, but 5 mol% C-LMO only shows one voltage plateau at the cutoff voltage as shown in Fig. 6. The discharge plateaus of C-LMO descend, and the two platforms integrate gradually during the recycling process. This may be due to that a small amount of Al<sup>3+</sup> embed into the crystal lattice of LiMn<sub>2</sub>O<sub>4</sub> and the stronger Al–O bond (bond energy of 512 kJ·mol<sup>-1</sup>) weakens Li–O bond (bond energy of 340.6 kJ·mol<sup>-1</sup>), making the lithium ions more easily spread the 8a-16c-8a channel, so the discharge performance of P-LMO samples is better [24]. However, the layer coated at calcined LiMn<sub>2</sub>O<sub>4</sub> does not have the above function, and the discharge capacity fades rapidly. This is in part due to the disproportionation reaction of Mn<sup>3+</sup> in the electrolyte:  $\text{Mn}^{3+}$  (insoluble)  $\rightarrow$   $\text{Mn}^{4+}$  (insoluble) + MnO (soluble). The dissolved Mn<sup>2+</sup> is reduced and deposited on the cathode surface in the form of

**Table 1** Initial specific discharge capacities of LMO, C-LMO, and P-LMO at 0.1C (mAh·g<sup>-1</sup>)

LMO	C-LMO-2	P-LMO-2	C-LMO-5	P-LMO-5
110.2	110.6	114.0	107.0	109.5

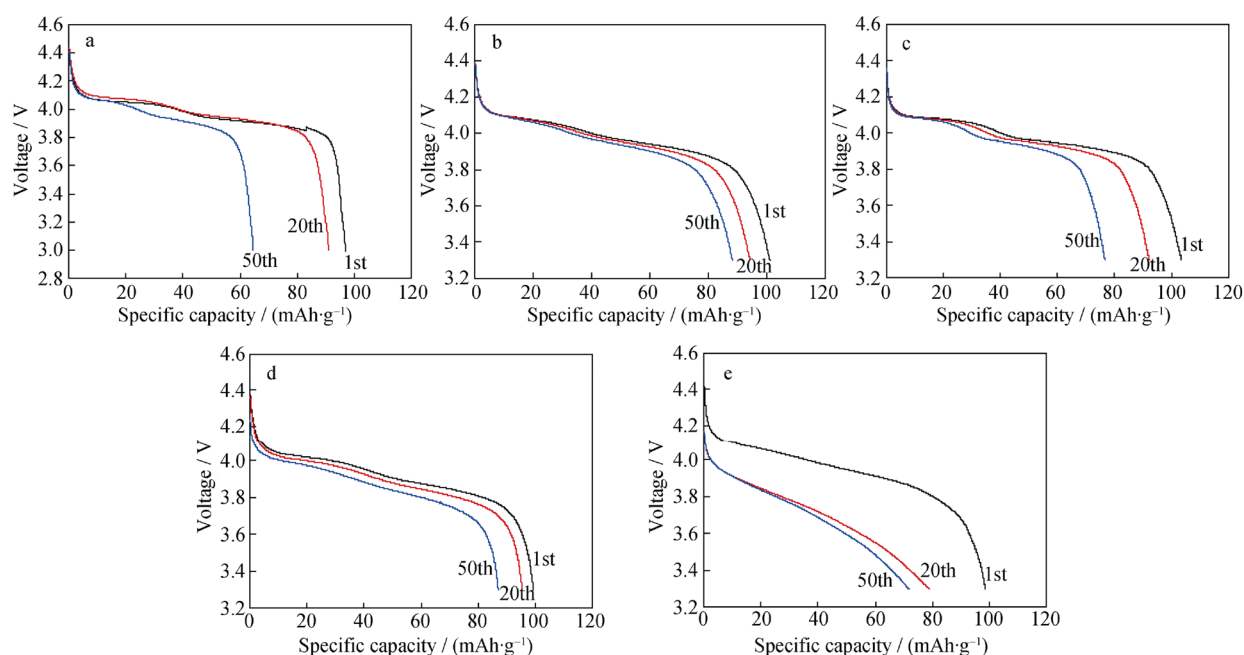


**Fig. 6** Discharge curves of pristine  $\text{LiMn}_2\text{O}_4$ - and  $\text{Al}_2\text{O}_3$ -coated  $\text{LiMn}_2\text{O}_4$  in voltage of 3.3–4.5 V at 0.5C: **a** LMO, **b** P-LMO-2, **c** C-LMO-2, **d** P-LMO-5, and **e** C-LMO-5

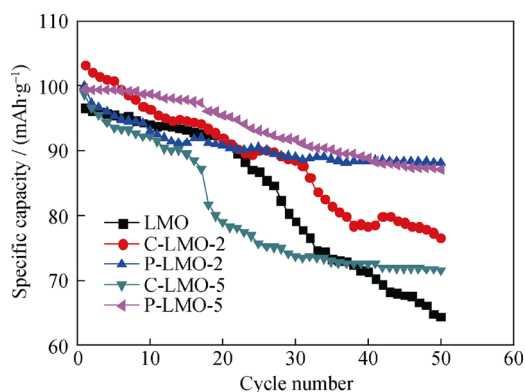


**Fig. 7** Cycling performances of LMO, C-LMO, and P-LMO in voltage of 3.3–4.5 V by applying a current of 0.5C at 55 °C

manganese, which leads to the increase of resistance. And the other part is that the excessive  $\text{Al}_2\text{O}_3$  seriously restrains the insertion and extraction of lithium ions with the increase of  $\text{Al}_2\text{O}_3$  coating amount. Both of them can cause polarization of the charge–discharge curves [25].

Figure 7 shows the cycling performances of LMO, C-LMO, and P-LMO in the voltage range of 3.3–4.5 V by applying a current of 0.5C at 55 °C. As for LMO, the specific discharge capacity fades from 96.7 to 64.4  $\text{mAh}\cdot\text{g}^{-1}$  after 50 cycles, with capacity loss of 33.4 %. In the case of P-LMO, the specific discharge capacities decrease from 100.9 to 88.1  $\text{mAh}\cdot\text{g}^{-1}$  and 99.5 to 86.8  $\text{mAh}\cdot\text{g}^{-1}$  with capacity loss of 12.7 % and 12.8 % for the coating contents of 2 mol% and 5 mol%, respectively. And

the capacity loss of corresponding C-LMO is 23.6 % and 27.5 %. Obviously, the cycling performance of P-LMO is superior to those of LMO and C-LMO material. It is attributed to the following reasons: (1) the layer coated at presintering period narrows the particle size range and facilitates the diffusion of lithium ions; (2) the small lattice constants help stabilize the structure of spinel crystal, and thus inhibiting the Jahn–Teller distortion accompanied by the change of electrode material from cubic to tetragonal; (3) the  $\text{Al}_2\text{O}_3$  layer helps improve the valence of Mn ions on the surface of (001) and can effectively reduce the dissolution of  $\text{Mn}^{3+}$  on the surface of the electrode as well as the chemical reaction between  $\text{Mn}^{3+}$  and electrolyte [26]. In addition, researches show that P-LMO-2 has a better cycle performance than P-LMO-5, which is due to that the excess  $\text{Al}_2\text{O}_3$  coated at P-LMO-5 will hinder the transportation of lithium ions, leading to the evident decay of the specific capacity.

In order to further understand the difference in their cyclic performance, electrochemical impedance spectroscopy (EIS) of pristine  $\text{LiMn}_2\text{O}_4$ - and  $\text{Al}_2\text{O}_3$ -coated  $\text{LiMn}_2\text{O}_4$  at the 1st cycle and 50th cycle were measured as shown in Fig. 8. Figure 8a shows the equivalent circuit of the cell to simulate film resistance ( $R_f$ ), charge transfer resistance ( $R_{ct}$ ), Warburg resistance ( $Z_w$ ), and capacitor element ( $CPE$ ). The  $R_f$  and  $R_{ct}$  data are listed in Table 2. From the results of the 1st cycle, the  $R_f$  values of P-LMO and C-LMO are larger than that of LMO due to the combination of the solid electrolyte interface (SEI) and  $\text{Al}_2\text{O}_3$

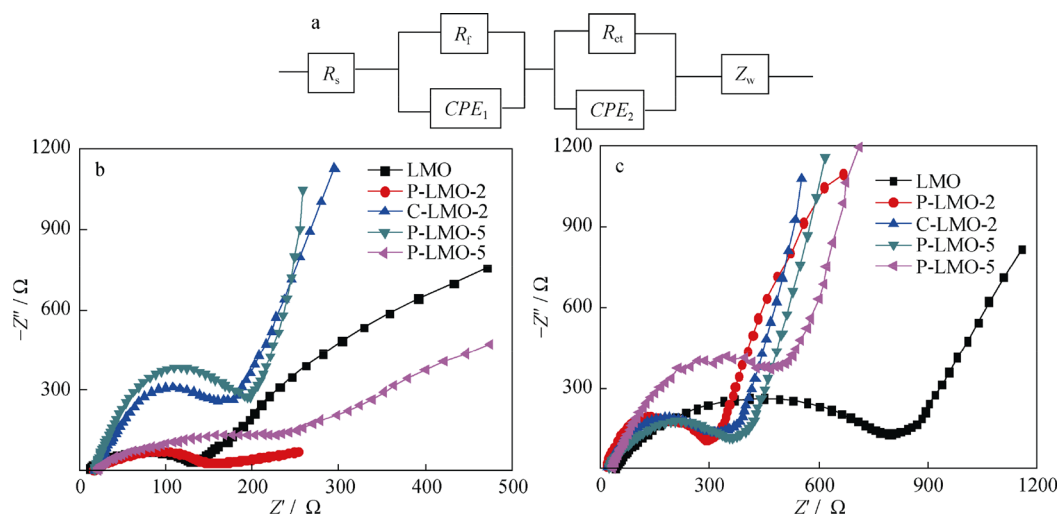


**Fig. 8** Equivalent circuit of cell **a** and EIS results of pristine LiMn<sub>2</sub>O<sub>4</sub>- and Al<sub>2</sub>O<sub>3</sub>-coated LiMn<sub>2</sub>O<sub>4</sub> at **b** 1st cycle and **c** 50th cycle

**Table 2**  $R_f$  and  $R_{ct}$  calculation of pristine LiMn<sub>2</sub>O<sub>4</sub>- and Al<sub>2</sub>O<sub>3</sub>-coated LiMn<sub>2</sub>O<sub>4</sub> at both 1st and 50th cycle based on equivalent circuit of the cell

Resistance	Cycle	LMO	P-LMO-2	C-LMO-2	P-LMO-5	C-LMO-5
$R_f/\Omega$	1st cycle	11.5	15.6	17.4	17.9	20.8
	50th cycle	42.6	19.2	22.5	24.8	32.7
$R_{ct}/\Omega$	1st cycle	134.5	151.1	160.3	180.1	213.7
	50th cycle	781.0	295.6	364.8	398.5	496.4

coating layer on the surface of LiMn<sub>2</sub>O<sub>4</sub>. The charge transfer resistance ( $R_{ct}$ ) of P-LMO has the slowest growth rate; and when the Al<sub>2</sub>O<sub>3</sub> coating amount is 5 mol%, the  $R_{ct}$  grows rapidly for both P-LMO and C-LMO. Similar situations appear in the results of the 50th cycle. This is mainly due to the dissolution of Mn ions, declining the instability of the spinel structure and further resulting in a rapid increase in impedance. However, the Al<sub>2</sub>O<sub>3</sub> coating layer at the surface of LiMn<sub>2</sub>O<sub>4</sub> can separate electrolytes and active materials to decrease the decomposition of electrolyte. Particularly, the LiAl<sub>y</sub>Mn<sub>2-y</sub>O<sub>4</sub> formed on the LiMn<sub>2</sub>O<sub>4</sub> surface in the P-LMO power strengthens the spinel structure and further decreases the growth rate of resistance. In addition, the excess Al<sub>2</sub>O<sub>3</sub> coated at P-LMO and C-LMO will hinder the transportation of lithium ions, leading to the rise of resistance.

In Fig. 9a and b, the CV profiles of Li/P-LMO-2 were compared with the Li/C-LMO-2 cells in the 1st and 50th cycles at room temperature. Figure 9 indicates that the intervals between the oxidation and the corresponding reduction potential of P-LMO are smaller than those of the C-LMO, indicating that the polarization of the cathode material decreases. CVs for the Li/C-LMO-2 show a distinct shift and broadening of the oxidation and reduction peaks during cycling, indicating a change in the surface

structure and composition of the spinel electrode. These changes are likely associated with the rapid capacity losses. By contrast, the CVs of Li/P-LMO-2 show significantly less peak shift and broadening, implying a quick electrode reaction after Al<sub>2</sub>O<sub>3</sub> pre-coated. The results are consistent with our conclusion that the Al<sub>2</sub>O<sub>3</sub> pre-coating plays an important role in protecting the electrode surface from chemical attack by acidic electrolyte species, such as HF; thereby, the structural and chemical character of the electrode surface are maintained. In addition, the CVs of C-LMO products appear a redox peak among the voltage of 3.1–3.2 V, while it does not occur in the pre-coated ones. This is mainly attributed to the aluminum hydroxide layer coated at the surface of presintered LiMn<sub>2</sub>O<sub>4</sub>. The layer can effectively avoid the generation of oxygen defects at a high temperature during the calcination process.

AAS results for the Mn dissolution of LMO, C-LMO, and P-LMO cathode materials are given in Fig. 10. The dissolved Mn contents of P-LMO and C-LMO are much lower than that of LMO powers, and that of the P-LMO is the lowest. As a result, it is demonstrated that both calc-coating and pre-coating of Al<sub>2</sub>O<sub>3</sub> could effectively reduce the dissolution of Mn from the electrode, but the solution-based Al<sub>2</sub>O<sub>3</sub> pre-coating is more effective in the reduction of the Mn dissolution into the electrolyte.

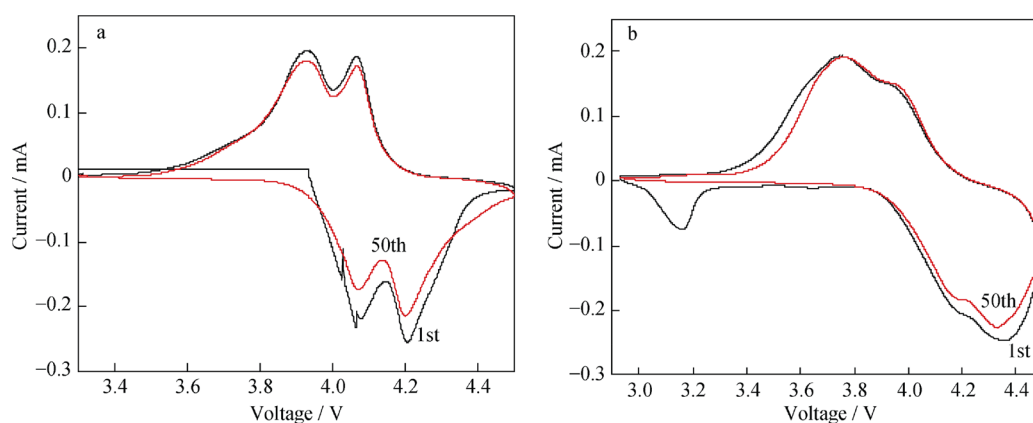


**Fig. 9** CV curves of **a** P-LMO-2 and **b** C-LMO-2 at different cycles measured at room temperature

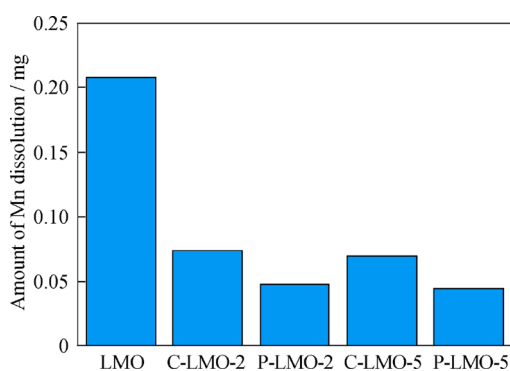


**Fig. 10** AAS results of pristine  $\text{LiMn}_2\text{O}_4$ - and  $\text{Al}_2\text{O}_3$ -coated  $\text{LiMn}_2\text{O}_4$  spinel cathode materials immersed in  $\text{LiPF}_6$  with EC/DEC volume ratio of 1:1

### 3.3 Mechanism exploration

Some researchers believed that the fast capacity loss during cycling for spinel  $\text{LiMn}_2\text{O}_4$  was mainly ascribed to the dissolution of manganese from the electrode. HF generated during cycling when using  $\text{LiPF}_6$ -based electrolyte was responsible for the dissolution of the manganese. This chemical reaction was proposed by Myung et al. [27]:



HF continuously attacks the active cathode material, and cathode material decomposes as the cycle goes by [28], causing capacity fading



Therefore, it is believed that the uniform layer coated at spinel  $\text{LiMn}_2\text{O}_4$  can effectively prevent cathode materials from direct contacting with the electrolyte, reduce the formation of HF, and greatly decrease the capacity loss. The electrochemical data obtained in this study demonstrate that the cycling performance of  $\text{LiMn}_2\text{O}_4$  electrode is significantly improved by pre-coating  $\text{Al}_2\text{O}_3$  layer. The layer coated at the surface of presintered  $\text{LiMn}_2\text{O}_4$  can

inhibit the growth of  $\text{LiMn}_2\text{O}_4$  during the further process of calcination and reduce the particle sizes. The small size is contributed to the diffusion of lithium ions. Owing to the decrease of diffusion distance, the utilization of the active material is improved. And P-LMO can also avoid the shortcoming of traditional C-LMO obtained by coating calcined  $\text{LiMn}_2\text{O}_4$ , in which the particles near the center of active materials are difficult to use. Moreover, the  $\text{Al}_2\text{O}_3$  layer can effectively decrease the interface area between the cathode and the electrolyte as well as the HF content at the cathode surface.

Pre-coating the spinel  $\text{LiMn}_2\text{O}_4$  with  $\text{Al}_2\text{O}_3$  layer via chemical deposition method results in the improvement of the electrochemical properties.

## 4 Conclusion

Spinel  $\text{LiMn}_2\text{O}_4$  was synthesized by the two-process solid-state method, and the  $\text{Al}_2\text{O}_3$  coating layer was coated on the surface of presintering  $\text{LiMn}_2\text{O}_4$  and calcined  $\text{LiMn}_2\text{O}_4$  by chemical deposition method.  $\text{Al}_2\text{O}_3$  layer forms uniformly on the surface of spinel  $\text{LiMn}_2\text{O}_4$ . Compared with C-LMO, P-LMO materials have smaller particle size and show much better capacity retention at 55 °C, especially the 2 mol%  $\text{Al}_2\text{O}_3$  pre-coated  $\text{LiMn}_2\text{O}_4$ . The capacity retention of this material is 87.3 % after 50 cycles. The surface modification with  $\text{Al}_2\text{O}_3$  coated at presintering period in this work acts at least two roles: (1) preventing the particles further excessively growing and facilitating the diffusion of lithium ions through it, and (2) separating electrolytes and active materials and thus preventing the dissolution of the Mn ions to ensure the structure stability. Furthermore, this pre-coated way combined with traditional solid-state method makes the industrialization of cathode material  $\text{LiMn}_2\text{O}_4$  for lithium-ion batteries more prosperous.

**Acknowledgments** This study was financially supported by the Science and Technology Project of Hunan Province (No. 2010FJ4061) and the Technology Project of Changsha (No. K1201039-11).

**Open Access** This article is distributed under the terms of the Creative Commons Attribution License which permits any use, distribution, and reproduction in any medium, provided the original author(s) and the source are credited.

## References

- [1] Xu B, Qian DN, Wang ZY, Meng YS. Recent progress in cathode materials research for advanced lithium ion batteries. *Mater Sci Eng.* 2012;73(5–6):51.
- [2] Wu HM, Tu JP, Chen XT, Li Y, Zhao XB, Cao GS. Electrochemical study on LiMn<sub>2</sub>O<sub>4</sub> as cathode material for lithium ion batteries. *J Electroanal Chem.* 2006;586(2):180.
- [3] He XM, Li JJ, Cai Y, Jiang CY, Wan CR. Preparation of spherical spinel LiMn<sub>2</sub>O<sub>4</sub> cathode material for Li-ion batteries. *Mater Chem Phys.* 2006;95(1):105.
- [4] Cabana J, Valdes-Solis T, Palacin MR, Oro-Sole J, Fuertes A, Marban G, Fuertes AB. Enhanced high rate performance of LiMn<sub>2</sub>O<sub>4</sub> spinel nanoparticles synthesized by a hard-template route. *J Power Sources.* 2007;166(2):492.
- [5] Li XF, Xu YL, Wang CL. Suppression of Jahn-Teller distortion of spinel LiMn<sub>2</sub>O<sub>4</sub> cathode. *J Alloy Compd.* 2009;479(1–2):310.
- [6] Xiao LF, Zhao YQ, Yang YY, Cao YL, Ai XP, Yang HX. Enhanced electrochemical stability of Al-doped LiMn<sub>2</sub>O<sub>4</sub> synthesized by a polymer-pyrolysis method. *Electrochim Acta.* 2008;54(2):545.
- [7] Xia YG, Wang HY, Zhang Q, Nakamura H, Noguchi H, Yoshio M. Oxygen deficiency, a key factor in controlling the cycle performance of Mn-spinel cathode for lithium-ion batteries. *J Power Sources.* 2007;166(2):485.
- [8] Oh SH, Chung KY, Jeon SH, Kim CS, Cho WB. Structural and electrochemical investigations on the LiNi<sub>0.5-x</sub>Mn<sub>1.5-y</sub>M<sub>x+y</sub>O<sub>4</sub> (M = Cr, Al, Zr) compound for 5 V cathode material. *J Alloy Compd.* 2009;469(1–2):244.
- [9] Hwang BJ, Tsai YW, Santhanam R, Wu YW, Hu SG, Lee JF, Liu DG. Evolution of local electronic and atomic structure of Co-doped LiMn<sub>2</sub>O<sub>4</sub> cathode material for lithium rechargeable batteries. *J Power Sources.* 2006;123(2):206.
- [10] Hwang BJ, Santhanam R, Liu DG, Tsai YW. Effect of Al-substitution on the stability of spinel LiMn<sub>2</sub>O<sub>4</sub> synthesized by citric acid sol-gel method. *J Power Sources.* 2001;102(1–2):326.
- [11] Wei YJ, Nam KW, Kim KB, Chen G. Spectroscopic studies of the structural properties of Ni substituted spinel LiMn<sub>2</sub>O<sub>4</sub>. *Solid State Ion.* 2006;177(1–2):29.
- [12] Lee KS, Bang HJ, Myung ST, Prakash J, Amine K, Sun YK. Synthesis and electrochemical properties of spherical spinel Li<sub>1.05</sub>M<sub>0.05</sub>Mn<sub>1.9</sub>O<sub>4</sub> (M = Mg and Al) as a cathode material for lithium-ion batteries by co-precipitation method. *J Power Sources.* 2007;174(2):726.
- [13] Walz KA, Johnson CS, Genthe J, Stoiber LC, Zeltner WA, Anderson MA, Thackeray MM. Elevated temperature cycling stability and electrochemical impedance of LiMn<sub>2</sub>O<sub>4</sub> cathodes with nanoporous ZrO<sub>2</sub> and TiO<sub>2</sub> coating. *J Power Sources.* 2010;195(15):4943.
- [14] Gnanaraj JS, Pol VG, Gedanken A, Aurbach D. Improving the high-temperature performance of LiMn<sub>2</sub>O<sub>4</sub> spinel electrodes by coating the active mass with MgO via a sonochemical method. *Electrochim Commun.* 2003;5(11):940.
- [15] Eftekhari A. Aluminum oxide as a multi-function agent for improving battery performance of LiMn<sub>2</sub>O<sub>4</sub> cathode. *Solid State Ion.* 2004;167(3–4):237.
- [16] Tu J, Zhao XB, Xie J, Cao GS, Zhuang DG, Zhu TJ, Tu JP. Enhanced low voltage cycling stability of LiMn<sub>2</sub>O<sub>4</sub> cathode by ZnO coating for lithium ion batteries. *J Alloy Compd.* 2007;432(1–2):313.
- [17] Ha HW, Yun NJ, Kim K. Improvement of electrochemical stability of LiMn<sub>2</sub>O<sub>4</sub> by CeO<sub>2</sub> coating for lithium-ion batteries. *Electrochim Acta.* 2007;52(9):3236.
- [18] Cui YL, Wu C, Wei T, Shi YL, Zhuang QC, Sun Z. Electrochemical performance of spinel LiMn<sub>2</sub>O<sub>4</sub> modified. *Hemistry.* 2011;74(8):742.
- [19] Tu J, Zhao XB, Cao GS, Zhuang DG, Zhu TJ, Tu JP. Enhanced cycling stability of LiMn<sub>2</sub>O<sub>4</sub> by surface modification with melting impregnation method. *Electrochim Acta.* 2006;51(28):6456.
- [20] Kim WK, Han DW, Ryu WH, Lim SJ, Kwon HS. Al<sub>2</sub>O<sub>3</sub> coating on LiMn<sub>2</sub>O<sub>4</sub> by electrostatic attraction forces and its effects on the high temperature cyclic performance. *Electrochim Acta.* 2012;71(5):17.
- [21] Halil S, Huseyin G, Saban P, Ahmet U. The effect of LBO coating method on electrochemical performance of LiMn<sub>2</sub>O<sub>4</sub> cathode material. *Solid State Ion.* 2008;178(35–36):1837.
- [22] Zheng ZQ. *Fundamentals of Materials Science.* Changsha: Central South University; 2005. 365.
- [23] Wang ZX, Xing ZJ, Li XH, Guo HJ, Peng WJ. Study on Al<sub>2</sub>O<sub>3</sub>-modified LiMn<sub>2</sub>O<sub>4</sub> prepared by heterogeneous nucleation. *Acta Phys Chim Sin.* 2004;20(8):790.
- [24] Xiong LL, Xu YL, Zhang C, Tao T. Doping-coating surface modification of spinel LiMn<sub>2</sub>O<sub>4</sub> cathode material with Al<sup>3+</sup> for lithium-ion batteries. *Acta Phys Chim Sin.* 2012;28(5):1177.
- [25] Duan F, Du ZZ, Yang P, Chen P, Zhong SS, Zhang DW. Study of coated as a cathode material for lithium ion batteries. *J Hefei Univ Technol (Nat Sci).* 2013;36(3):346.
- [26] Li XC, Zhang XY, Lu YJ, Li K. Interface reaction mechanism of welding Al<sub>2</sub>O<sub>3</sub> ceramic with AgCuInTi brazing filler. *Chin J Rare Met.* 2013;37(1):71.
- [27] Myung ST, Izumi K, Komaba S, Sun YK, Yashiro H, Kumagai N. Role of alumina coating on Li-Ni-Co-Mn-O particles as positive electrode material for lithium-ion batteries. *Chem Mater.* 2005;17(14):3695.
- [28] Qing CB, Bai Y, Yang JM, Zhang WF. Enhanced cycling stability of LiMn<sub>2</sub>O<sub>4</sub> cathode by amorphous FePO<sub>4</sub> coating. *Electrochim Acta.* 2011;56(19):6612.